

Communication

# Design of a Hybrid Split-Delay Line for Hard X-ray Free-Electron Lasers

Yihui Xu <sup>1,2</sup>, Chen Wu <sup>3</sup>, Jiadong Fan <sup>1,2</sup>, Zhen Wang <sup>1,2</sup>, Yajun Tong <sup>1,2</sup>, Qiushi Huang <sup>4</sup> , Chuan Yang <sup>5</sup>, Xiaohao Dong <sup>2,6</sup>, Huidong Jiang <sup>1,2,\*</sup> and Zhi Liu <sup>1,2</sup>

- <sup>1</sup> Center for Transformative Science, ShanghaiTech University, 393 Middle Huaxia Road, Shanghai 201210, China; xuyh1@shanghaitech.edu.cn (Y.X.); fanjd@shanghaitech.edu.cn (J.F.); wangz@shanghaitech.edu.cn (Z.W.); tongyj@shanghaitech.edu.cn (Y.T.); liuzhi@shanghaitech.edu.cn (Z.L.)
- <sup>2</sup> Shanghai High Repetition Rate XFEL and Extreme Light Facility, 393 Middle Huaxia Road, Shanghai 201210, China; dongxiaohao@zjlab.org.cn
- <sup>3</sup> School of Physical Science and Technology, ShanghaiTech University, 393 Middle Huaxia Road, Shanghai 201210, China; wuchen@shanghaitech.edu.cn
- <sup>4</sup> School of Physics Science and Engineering, Tongji University, 1239 Siping Road, Shanghai 200092, China; huangqs@tongji.edu.cn
- <sup>5</sup> Institute of Advanced Science Facilities, 268 Zhengyuan Road, Shenzheng 518107, China; yangc@mail.iasf.ac.cn or chuanyang@mail.iasf.ac.cn
- <sup>6</sup> Shanghai Advanced Research Institute, Chinese Academy of Sciences, 99 Haik Road, Shanghai 201210, China
- \* Correspondence: jianghd@shanghaitech.edu.cn

**Abstract:** High repetition-rate X-ray free-electron lasers (XFELs) enable the study of fast dynamics on microsecond time scales. Split-delay lines (SDLs) further bring the time scale down to femtoseconds by splitting and delaying the XFEL pulses. Crystals and multilayers are two common types of optical elements in SDLs, offering either long delay ranges or high temporal accuracy. In this work, we introduce the design of a hybrid SDL for the coherent diffraction endstation of Shanghai High Repetition Rate XFEL and Extreme Light Facility (SHINE). It uses crystals for the first branch and multilayers for the second one, thus simultaneously offering a relatively long delay range and high temporal accuracy. Moreover, a third branch can be installed to switch the SDL to the all-crystal configuration for longer delay ranges.

**Keywords:** XFEL; split-delay line; XPCS; hybrid; wavefront propagation



**Citation:** Xu, Y.; Wu, C.; Fan, J.; Wang, Z.; Tong, Y.; Huang, Q.; Yang, C.; Dong, X.; Jiang, H.; Liu, Z. Design of a Hybrid Split-Delay Line for Hard X-ray Free-Electron Lasers. *Photonics* **2022**, *9*, 136. <https://doi.org/10.3390/photonics9030136>

Received: 30 December 2021

Accepted: 13 January 2022

Published: 26 February 2022

**Publisher's Note:** MDPI stays neutral with regard to jurisdictional claims in published maps and institutional affiliations.



**Copyright:** © 2022 by the authors. Licensee MDPI, Basel, Switzerland. This article is an open access article distributed under the terms and conditions of the Creative Commons Attribution (CC BY) license (<https://creativecommons.org/licenses/by/4.0/>).

## 1. Introduction

Hard X-ray free-electron lasers (XFELs) provide ultra-short, ultra-bright, and highly coherent X-ray pulses in the hard X-ray regime [1]. Among them, high repetition-rate facilities such as the European XFEL enable the study of fast dynamics on microsecond time scales [2]. Split-delay lines (SDLs) can further bring the time scale down to femtoseconds by splitting and delaying the XFEL pulses [3]. Moreover, SDLs can be used as autocorrelators to characterize the coherence properties [4,5]. There are two common types of optical elements for SDLs, namely crystals and multilayers [6,7]. Crystal-based SDLs offer up-to-nanosecond delay ranges [8,9], but relatively low accuracy. In contrast, multilayer-based SDLs offer sub-femtosecond temporal accuracy but limited delay ranges [10].

Shanghai High Repetition Rate XFEL and Extreme Light Facility (SHINE) is the first hard X-ray XFEL project in China. It will employ a superconducting LINAC to produce ultrashort XFEL pulses at 1 MHz continuously [11]. The coherent diffraction endstation (CDE) at SHINE aims at ultrafast dynamics using scattering and imaging methods such as X-ray photon correlation spectroscopy (XPCS) and coherent diffractive imaging (CDI). An SDL system is required to probe sub-microsecond dynamics using methods such as split-delay XPCS [3] and sequential imaging [12]. Here we report the design of a hybrid SDL, which uses crystals for the first branch and multilayers for the second, featuring

a relatively long delay range and high accuracy simultaneously. Thanks to the vertical polarization of the beamline, the hybrid SDL will adopt a horizontal layout. Therefore, it is possible to install a third branch and switch to the all-crystal configuration when longer delays are desired.

## 2. Conceptual Design

### 2.1. Beamline and SDL Design

As shown in Figure 1a, focusing is achieved by two sets of compound refractive lenses (CRLs). Between the CRLs, a retractable monochromator composed of 4 Si111 crystals is installed. The SDL locates 23.5 m downstream CRL2 and 4 m upstream the focus. In the early phase of operation, the beamline will deliver 10–15 keV pulses, which is also the main operating range of the SDL.

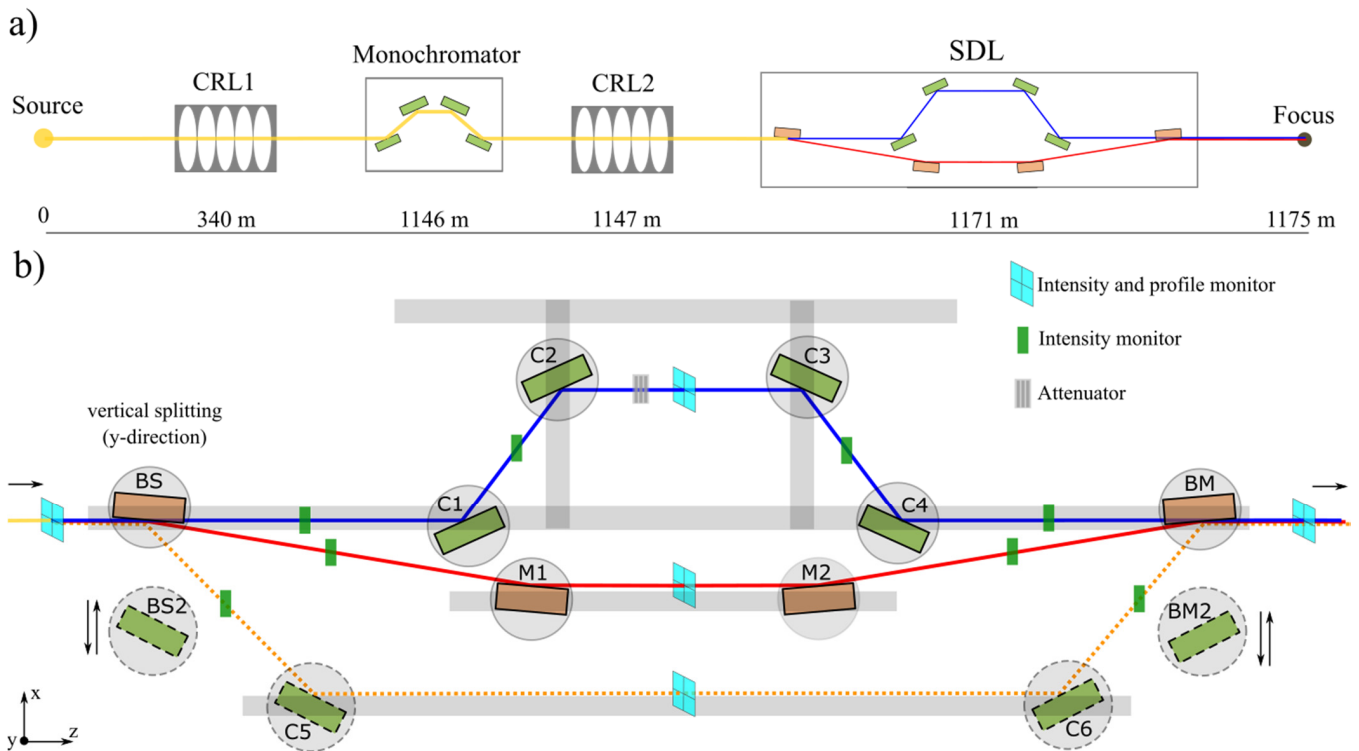


**Figure 1.** (a) Beamline layout of the CDE endstation. CRL1 is used to collimate the beam and CRL2 to focus the beam. The retractable monochromator is composed of 4 Si111 crystals. (b) Top-view illustration of the hybrid SDL. BS denotes the beam splitter, BM the beam merger, C1–C6 crystals, M1–M2 multilayers, BS2 the spare beam splitter, and BM2 the spare beam merger. The dashed lines denote the beam path of the optional third branch. All stages (circular region) can slide along the guide rails (shadowed region).

Due to the difficulty in the fabrication of high-quality thin crystals, and the thermal deformation at high heat load [8], the hybrid SDL uses the wavefront splitting scheme to split the beam. As shown in Figure 1b, the entire system lies horizontally on an optical table (the x–z plane). The multilayer beam splitter (BS) splits the XFEL pulses vertically into two sub-pulses (in the y-direction). For this purpose, the effective part of the BS and BM are half as tall as that of the others. After BM, the sub-pulses travel either via the first branch composed of 4 silicon crystals (C1–C4) or the second branch composed of two multilayers (M1–M2). Their path length can be varied by sliding the stages (circular region) along the guide rails (shadowed paths), or by moving the stages via their x- and z-freedom. Eventually, the sub-pulses are merged by the multilayer beam merger (BM).

The hybrid SDL employs a horizontal layout due to the vertical polarization of the beamline, which is the same as that of the HXU at LCLS-II [8]. This enables additional

branches alongside the existing ones. Specifically, a third branch (the dashed path in Figure 1b) composed of 4 crystals will be installed. When longer delays are desired, the SDL can operate in the all-crystal configuration using the first and the third branch. To this end, the multilayer-based BS and BM will be replaced by the crystal-based BS2 and BM2.

### 2.2. Crystals and Multilayers

Si111 crystals and W/B<sub>4</sub>C multilayers with a periodicity of 1.96 nm are selected for the hybrid SDL [10]. This combination ensures an acceptable minimum delay, as shown in the next section. Another reason for Si111 is its relatively large bandwidth, allowing for shorter pulses compared with higher-index Si such as Si220 and Si311. Due to the Fourier-transform limit, at 10 keV the XFEL pulses are longer than 1.40 fs for Si111, 3.18 fs for Si220, and 6.75 fs for Si311. To obtain sub-femtosecond resolution, one can either retract C1 and C4 to allow the upper sub-pulses to pass directly or implement an all-multilayer configuration. The latter is one of our future tasks. In both cases, the monochromator shall be retracted.

The effective surface area of the crystals is 25 mm × 5 mm (H × V), whereas that of the multilayers is 50 mm × 5 mm. Both of them largely exceed the footprint size of the beam on them at 10–15 keV.

The expected roughness of the crystals is about 2 Å, whereas that of the multilayers is about 3 Å. The resulting overall transmission at 10 keV is about 47% for crystals and 11% for multilayers. Therefore, a solid attenuator is implemented in the first branch to obtain sub-pulses of comparable flux.

### 2.3. The Delay Range

Below we calculate the delay range using the geometry in the literature assuming an infinitely-narrow beam [13]. The path length difference is obtained by subtracting the longitudinal length from the beam path length for each branch. The maximum delay is calculated by

$$\tau_{max} = \frac{(1.6 \text{ m} - 0.2 \text{ m}) \times \left(\frac{1}{\cos 2\theta_C} - 1\right) - 1.7 \text{ m} \times \left(\frac{1}{\cos 2\theta_M} - 1\right)}{c} \quad (1)$$

where 1.6 m is the maximum distance between C1 and C4, 0.2 m the minimum distance between C2 and C3, 1.7 m the minimum distance between BS and BM,  $\theta_C$  the Bragg angle of crystals,  $\theta_M$  the Bragg angle of multilayers,  $c$  the speed of light. The minimum delay is calculated by

$$\tau_{min} = \frac{\frac{2 \text{ mm}}{\sin \theta_C} \times (1 - \cos 2\theta_C) \times 2 - 2 \text{ m} \times \left(\frac{1}{\cos 2\theta_M} - 1\right)}{c} \quad (2)$$

where 2 mm is the minimum surface distance between C1 and C2 (also C3 and C4), and 2 m the maximum distance between BS and BM.

Figure 2 shows the calculated maximum and minimum delays of the SDL in the photon energy range of 10–15 keV. As expected, both  $\tau_{max}$  and  $\tau_{min}$  decrease with the photon energy. At 10 keV we obtain  $\tau_{max} \approx 384$  ps and at 15 keV we obtain  $\tau_{max} \approx 163$  ps, which shall be sufficient for most split-delay experiments [14–16]. In contrast,  $\tau_{min}$  is rather limited but still workable. Both  $\tau_{max}$  and  $\tau_{min}$  can be increased by switching to the all-crystal configuration.

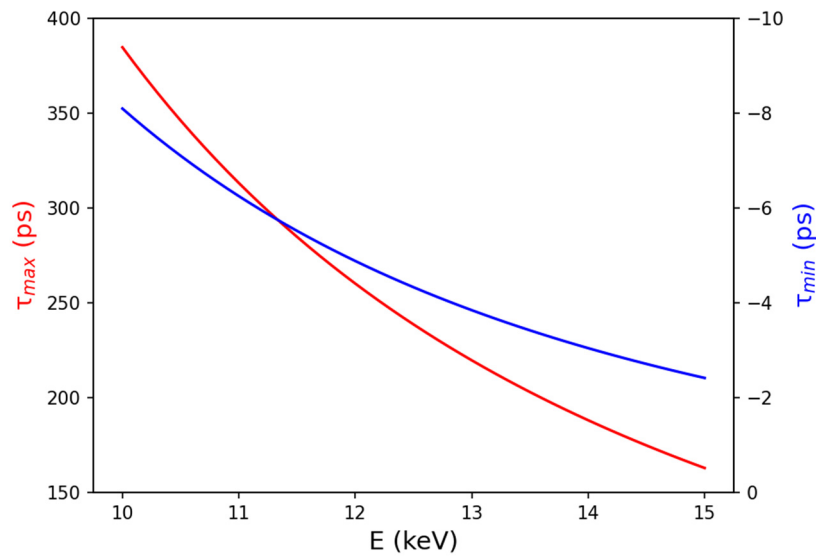


**Figure 2.** Calculated maximum and minimum delays of the hybrid SDL in the photon energy range of 10–15 keV.

2.4. The Temporal Accuracy

One of the advantages of this hybrid design is the high temporal accuracy. Under good surface alignment and high stability [13,17], it is determined by the translational motion accuracy along the beam [6,10]. It equals  $\Delta L / \sin 2\theta_C$  for crystals and  $\Delta L / \sin 2\theta_M$  for multilayers, where  $\Delta L \leq \pm 1 \mu\text{m}$  is the translational accuracy in the x- and z-directions [9]. For an infinitely narrow beam, the temporal accuracy can be calculated by

$$\Delta\tau_C = \frac{2 \times \frac{\Delta L}{\sin 2\theta_C} \times (1 - \cos 2\theta_C)}{c} \tag{3}$$

for crystals, and

$$\Delta\tau_M = \frac{2 \times \frac{\Delta L}{\sin 2\theta_M} \times (1 - \cos 2\theta_M)}{c} \tag{4}$$

for multilayers. At 10 keV,  $\Delta\tau_C \leq 1.34 \text{ fs}$  and  $\Delta\tau_M \leq 0.21 \text{ fs}$ . At higher photon energies, higher temporal accuracy is expected. The temporal accuracy of crystals shall be sufficient for experiments requiring long pulses or long delays. When performing split-delay in the low-charge (short-pulse) mode [14,18], the temporal accuracy of multilayers is highly advantageous.

2.5. Beam Overlapping

In the wavefront splitting scheme, there is a small gap between the sub-pulses due to knife-edge diffraction from the edges of the BM and BS [19]. Full overlap can be achieved either by focusing or by slightly tuning the crystals/multilayers [10,19]. At CDE, the focusing elements ensure the overlap at the focus but not at other positions.

Tuning the multilayers can be performed in a large angular range due to its large Darwin width (488.69  $\mu\text{rad}$  at 10 keV). This helps to fully overlap the beam at multiple positions rather than only at the focus. Likewise, non-collinear merging can be achieved without additional mirrors [9].

3. Technical Design

3.1. System Layout

As illustrated in Figure 3, the multilayers and crystals are mounted on 5-axis motor stages, which provide x, y, z, pitch, and roll freedom. All stages can slide along the guide rails. In addition, the C2 and C3 stages can slide in the x-direction via cross guide rails. The linear motion of the multilayers in the x-direction is provided by the x-axis freedom

of the stages with an expected travel range of 30 mm, corresponding to a path length of about 0.5 m. All components will be hosted in a vacuum enclosure, which is supported separately from the optical table.

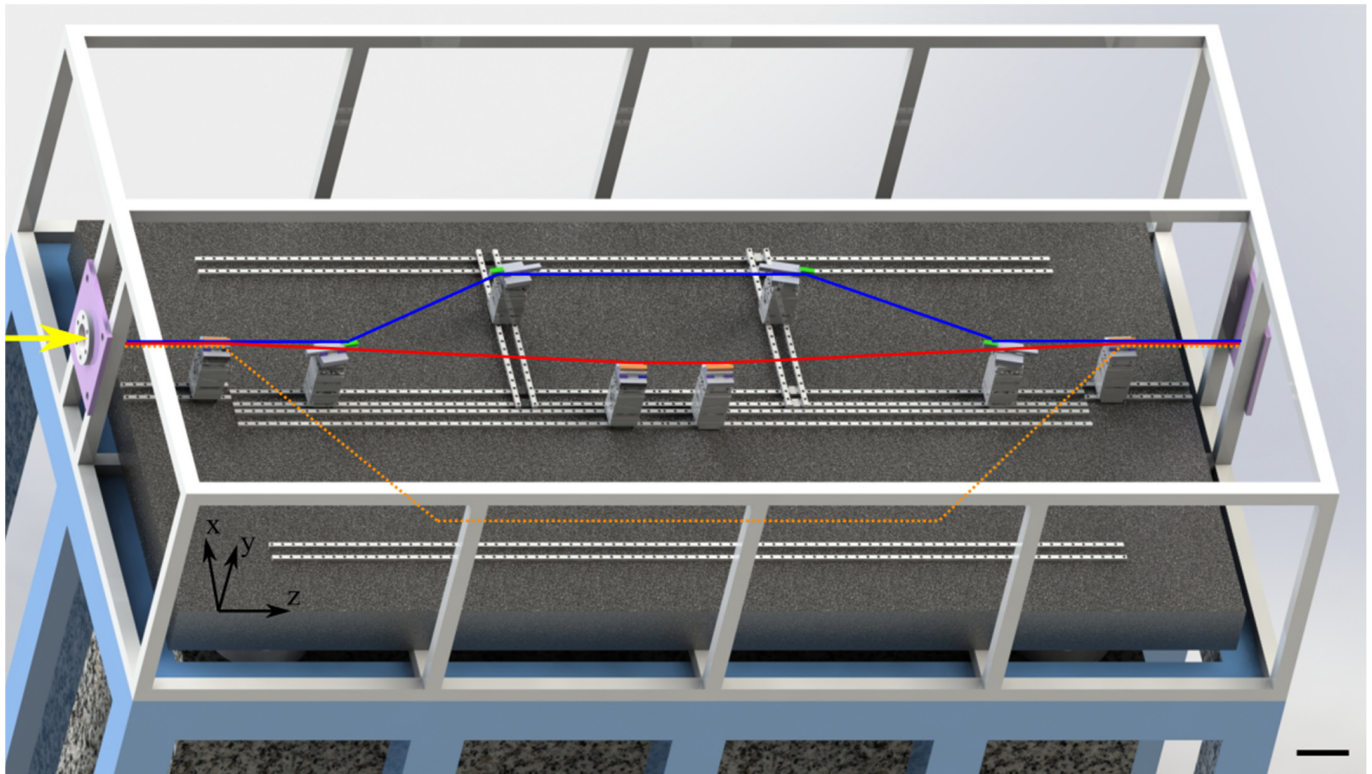


**Figure 3.** Illustrative mechanical layout of the hybrid SDL system. Colored lines are the paths of the (sub)pulses. The orange blocks illustrate the effective parts of the multilayers. Green blocks illustrate the effective parts of the crystals. The monitors and the attenuator are not shown for clarity. The black scale bar denotes 100 mm.

### 3.2. The Si Crystals

For acceptable negative delays, the minimum surface distance of C1–C2 and C3–C4 shall be less than 2 mm. To this end, a special design is applied to C1, C2, C3, and C4, similar to the channel-cut crystals of the SDL at LCLS [20]. In both designs, the base crystals stick out and the effective parts (shown in green in Figure 4) extrude from the base crystals. In this way, the collision of the motor stages no longer hinders the approaching of crystals.

### 3.3. The Heat Load

At 10 keV and 1 MHz in the high-charge mode with the monochromator employed, the expected maximum heat load at the BS is about 12 W, and that at C1 is about 6 W. The heat load will be about 5 times higher when the monochromator is retracted (pink beam). Therefore, the SDL cannot run at full power without cooling. In the early phase of operation, the effective pulse number and/or the effective repetition rate shall be constrained [21], such that significant thermal effects can be avoided. In the long run, a cooling system shall be implemented, for which the mechanical stability of the optics must be carefully assessed.

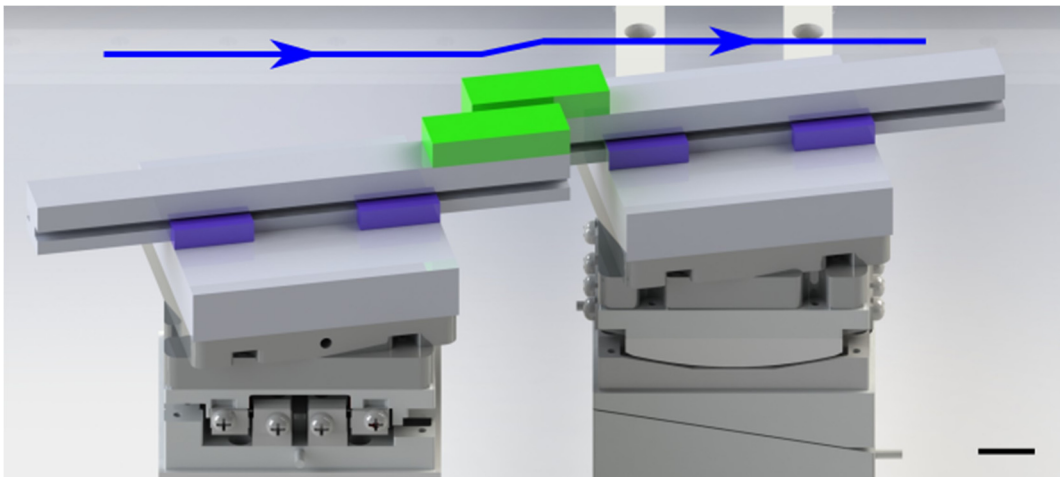


**Figure 4.** Illustrative mechanical layout of the C1 and C2 stages in the state of minimum surface distance. Green blocks illustrate the effective parts of the crystals. The blue lines above illustrate the beam path. The *SMARACT Modular System* is used for illustration. The black scale bar denotes 10 mm.

#### 4. Wavefront Propagation Simulation

Performance of the hybrid SDL was evaluated by the front-to-end simulation. For this purpose, wavefront propagation was performed using the SRW software package [22]. A self-coded python script merged the intensity and phase maps of both sub-pulses exported from SRW. Figure 5a shows the simulated beam profile on the plane 0.1 m downstream the SDL and 1.9 m upstream the focus. The edge diffraction fringes from the edges of BM and BS appear in both sub-pulses, leading to a gap between them [19]. The fringes in the upper part are stronger due to the higher transmission of crystals. The attenuator shall be inserted when equal sub-pulse energies are desired.

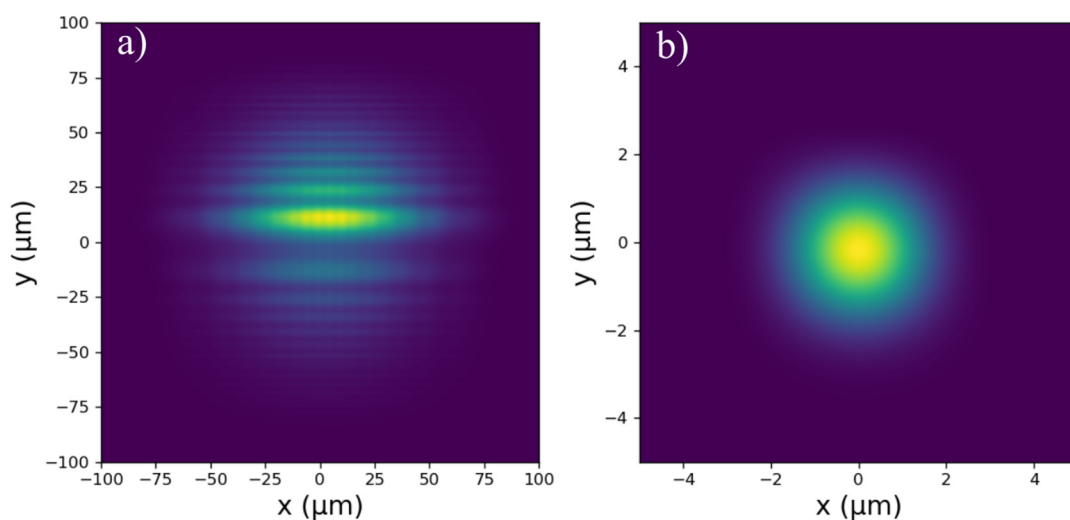


**Figure 5.** (a) Simulated transverse beam profile on the plane 0.1 m downstream the SDL and 1.9 m upstream the focus. (b) Simulated transverse beam profile on the focus plane when the attenuator is employed.

Figure 5b shows the simulated beam profile on the focus plane when the attenuator is employed. The Gaussian profile indicates a good overlap of the sub-pulses. No interference between sub-pulses is visible due to the large interference spacing (about 5  $\mu\text{m}$ ) [17].

## 5. Discussion

SDLs are powerful tools to explore ultrafast dynamics on sub-microsecond scales at XFELs. Therefore, an SDL is designed for the CDE endstation of SHINE, which mainly operates in the photon energy range of 10–15 keV. It will use Si111 crystals for the first branch and W/B<sub>4</sub>C multilayers for the second. The motivation of this hybrid design is to simultaneously provide a relatively long delay range and high temporal accuracy. Calculations show that the current design offers a delay range from −8 to 384 ps and the temporal accuracy better than 0.21 fs at 10 keV. Such a delay range is sufficient for most split-delay experiments [14–16], and the temporal accuracy is highly advantageous to those working in the low-charge mode [14,18]. Other essential technical aspects such as beam overlapping and the heat load are carefully considered. Wavefront propagation simulation further demonstrates the performance of the hybrid SDL [10,22]. Off the focus plane, the sub-pulses are separated by a small gap due to edge diffraction. On the focus plane, the sub-pulses largely overlap, resulting in a Gaussian profile.

Currently, most SDLs for hard X-ray XFELs are based on crystals [6,8,9,13], which offer delay ranges up to several nanoseconds. However, the temporal accuracy of crystal-based SDLs is limited to several femtoseconds due to the large diffraction angles. Moreover, crystals do not allow for attosecond pulses due to the Fourier-transform limit. Therefore, it is preferred to use multilayers for (sub-)femtosecond split-delay experiments. Multilayers provide small diffraction angles and larger bandwidth, thus enabling (sub-)femtosecond split and delay. This design has been successfully implemented at FLASH and is under development for the HED endstation at the European XFEL [10,17]. Our hybrid design is expected to integrate their advantages. Moreover, the hybrid SDL adopts a horizontal layout due to the vertical polarization. It is thus possible to install a third branch and switch to an all-crystal configuration for longer delays.

## 6. Conclusions

In this work, the design of a hybrid SDL designed for the CDE endstation of SHINE is introduced. By combining Si111 crystals and W/B<sub>4</sub>C multilayers, both a relatively long delay range and high temporal accuracy are available. Moreover, longer ranges can be achieved by switching to the all-crystal design using the first and the third branch. Its performance is demonstrated by wavefront propagation simulation.

In terms of future work, other critical components such as the cooling system, the laser interferometer system, and an optional all-multilayer configuration shall be carefully considered. The cooling system would enable higher-power operation, the laser interferometer would enable higher accuracy, and the all-multilayer configuration would enable sub-femtosecond split-delay.

**Author Contributions:** Investigation and conceptualization, Y.X., Y.T., J.F., Q.H. and X.D.; software, C.W., Z.W. and C.Y.; writing, Y.X.; correction and supervision, H.J. and Z.L.; funding acquisition, J.F. and H.J. All authors have read and agreed to the published version of the manuscript.

**Funding:** This work was sponsored by Natural Science Foundation of Shanghai (Grant No. 22ZR1442100), the Strategic Priority Research Program of Chinese Academy of Sciences (Grant No. XDB 37040303), the Major State Basic Research Development Program of China (2017YFA0504802), and the National Natural Science Foundation of China (Grant No. 21727817).

**Acknowledgments:** The authors thank Wei Lu from the European XFEL for the helpful discussions.

**Conflicts of Interest:** The authors declare no conflict of interest.

## References

1. Huang, Z.; Kim, K.-J. Review of X-ray free-electron laser theory. *Phys. Rev. ST Accel. Beams* **2007**, *10*, 034801. [[CrossRef](#)]
2. Dallari, F.; Reiser, M.; Lokteva, I.; Jain, A.; Möller, J.; Scholz, M.; Madsen, A.; Grübel, G.; Perakis, F.; Lehmkuhler, F. Analysis Strategies for MHz XPCS at the European XFEL. *Appl. Sci.* **2021**, *11*, 8037. [[CrossRef](#)]

3. Roseker, W.; Hruszkewycz, S.O.; Lehmkuhler, F.; Walther, M.; Schulte-Schrepping, H.; Lee, S.; Osaka, T.; Strüder, L.; Hartmann, R.; Sikorski, M.; et al. Towards ultrafast dynamics with split-pulse X-ray photon correlation spectroscopy at free electron laser sources. *Nat. Commun.* **2018**, *9*, 1704. [[CrossRef](#)] [[PubMed](#)]
4. Mitzner, R.; Siemer, B.; Neeb, M.; Noll, T.; Siewert, F.; Roling, S.; Rutkowski, M.; Sorokin, A.A.; Richter, M.; Juranic, P.; et al. Spatio-temporal coherence of free electron laser pulses in the soft x-ray regime. *Opt. Express* **2008**, *16*, 19909. [[CrossRef](#)] [[PubMed](#)]
5. Osaka, T.; Hirano, T.; Morioka, Y.; Sano, Y.; Inubushi, Y.; Togashi, T.; Inoue, I.; Tono, K.; Robert, A.; Yamauchi, K.; et al. Characterization of temporal coherence of hard X-ray free-electron laser pulses with single-shot interferograms. *IUCr* **2017**, *4*, 728–733. [[CrossRef](#)] [[PubMed](#)]
6. Roseker, W.; Franz, H.; Schulte-Schrepping, H.; Ehnes, A.; Leupold, O.; Zontone, F.; Lee, S.; Robert, A.; Grübel, G. Development of a hard X-ray delay line for X-ray photon correlation spectroscopy and jitter-free pump–probe experiments at X-ray free-electron laser sources. *J. Synchrotron. Rad.* **2011**, *18*, 481–491. [[CrossRef](#)] [[PubMed](#)]
7. Roling, S.; Zacharias, H. Split-and-Delay Units for Soft and Hard X-Rays. In *Synchrotron Light Sources and Free-Electron Lasers*; Jaeschke, E.J., Khan, S., Schneider, J.R., Hastings, J.B., Eds.; Springer International Publishing: Cham, Switzerland, 2020; pp. 1057–1091, ISBN 978-3-030-23200-9.
8. Zhu, D.; Sun, Y.; Schafer, D.W.; Shi, H.; James, J.H.; Gumerlock, K.L.; Osier, T.O.; Whitney, R.; Zhang, L.; Nicolas, J.; et al. Development of a Hard X-ray Split-Delay System at the Linac Coherent Light Source. In Proceedings of the Advances in X-ray Free-Electron Lasers Instrumentation IV (2017), Prague, Czech Republic, 25–27 April 2017; Tschentscher, T., Patthey, L., Eds.; SPIE Press: Prague, Czech Republic, 2017; p. 102370R.
9. Lu, W.; Friedrich, B.; Noll, T.; Zhou, K.; Hallmann, J.; Ansaldi, G.; Roth, T.; Serkez, S.; Geloni, G.; Madsen, A.; et al. Development of a hard X-ray split-and-delay line and performance simulations for two-color pump-probe experiments at the European XFEL. *Rev. Sci. Instrum.* **2018**, *89*, 063121. [[CrossRef](#)] [[PubMed](#)]
10. Roling, S.; Kärcher, V.; Samoylova, L.; Appel, K.; Braun, S.; Gawlitza, P.; Siewert, F.; Zastrau, U.; Rollnik, M.; Wahlert, F.; et al. A Hard X-ray Split-and-Delay Unit for the HED Instrument at the European XFEL. In Proceedings of the Advances in X-ray Free-Electron Lasers Instrumentation IV (2017), Prague, Czech Republic, 25–27 April 2017; Tschentscher, T., Patthey, L., Eds.; SPIE Press: Prague, Czech Republic, 2017; p. 1023713.
11. Huang, N.; Deng, H.X.; Liu, B.; Wang, D. Physical Design and FEL Performance Study for FEL-III Beamline of SHINE. In Proceedings of the 39th International Free Electron Laser Conference (FEL2019), Hamburg, Germany, 26–30 August 2019; JACoW Publishing: Geneva, Switzerland, 2019; pp. 199–202.
12. Günther, C.M.; Pfau, B.; Mitzner, R.; Siemer, B.; Roling, S.; Zacharias, H.; Kutz, O.; Rudolph, I.; Schondelmaier, D.; Treusch, R.; et al. Sequential femtosecond X-ray imaging. *Nat. Phot.* **2011**, *5*, 99–102. [[CrossRef](#)]
13. Osaka, T.; Hirano, T.; Sano, Y.; Inubushi, Y.; Matsuyama, S.; Tono, K.; Ishikawa, T.; Yamauchi, K.; Yabashi, M. Wavelength-tunable split-and-delay optical system for hard X-ray free-electron lasers. *Opt. Express* **2016**, *24*, 9187. [[CrossRef](#)]
14. Perakis, F.; Camisasca, G.; Lane, T.J.; Späh, A.; Wikfeldt, K.T.; Sellberg, J.A.; Lehmkuhler, F.; Pathak, H.; Kim, K.H.; Amann-Winkel, K.; et al. Coherent X-rays reveal the influence of cage effects on ultrafast water dynamics. *Nat. Commun.* **2018**, *9*, 1917. [[CrossRef](#)]
15. Schmidt, K.E.; Spence, J.C.H.; Weierstall, U.; Kirian, R.; Wang, X.; Starodub, D.; Chapman, H.N.; Howells, M.R.; Doak, R.B. Tomographic Femtosecond X-Ray Diffractive Imaging. *Phys. Rev. Lett.* **2008**, *11*, 115507. [[CrossRef](#)]
16. van Thor, J.J.; Madsen, A. A split-beam probe-pump-probe scheme for femtosecond time resolved protein X-ray crystallography. *Struct. Dyn.* **2015**, *2*, 014102. [[CrossRef](#)] [[PubMed](#)]
17. Mitzner, R.; Neeb, M.; Noll, T.; Pontius, N.; Eberhardt, W. An X-ray Autocorrelator and Delay Line for the VUV-FEL at TTF/DESY. In Proceedings of the Ultrafast X-Ray Detectors, High-Speed Imaging, and Applications, San Diego, CA, USA, 31 July–4 August 2005; SPIE: San Diego, CA, USA, 2005; p. 59200D.
18. Helml, W.; Grguraš, I.; Juranic, P.; Düsterer, S.; Mazza, T.; Maier, A.; Hartmann, N.; Ilchen, M.; Hartmann, G.; Patthey, L.; et al. Ultrashort Free-Electron Laser X-ray Pulses. *Appl. Sci.* **2017**, *7*, 915. [[CrossRef](#)]
19. Hirano, T.; Osaka, T.; Morioka, Y.; Sano, Y.; Inubushi, Y.; Togashi, T.; Inoue, I.; Matsuyama, S.; Tono, K.; Robert, A.; et al. Performance of a hard X-ray split-and-delay optical system with a wavefront division. *J. Synchrotron. Rad.* **2018**, *25*, 20–25. [[CrossRef](#)]
20. Shi, H.; Zhu, D. Multi-Axis Nanopositioning System for the Hard X-ray Split-Delay System at the LCLS. *Synchrotron. Radiat. News* **2018**, *31*, 15–20. [[CrossRef](#)]
21. Scholz, M. FEL Performance Achieved at European XFEL. *Free Electron Lasers* **2018**, *5*, 29–33.
22. Chubar, O.; Rakitin, M.S.; Chen-Wiegart, Y.-C.; Chu, Y.S.; Fluerasu, A.; Hidas, D.; Wiegart, L. Main functions, recent updates, and applications of Synchrotron Radiation Workshop code. In Proceedings of the Advances in Computational Methods for X-Ray Optics IV, San Diego, CA, USA, 9–10 August 2017; Sawhney, K., Chubar, O., Eds.; SPIE Press: San Diego, CA, USA, 2017; p. 1038805.